Homeostatic mechanisms regulate distinct aspects of cortical circuit dynamics

Yue Kris Wu[a], Keith B. Hengen[b,c], Gina G. Turrigiano[b,1], and Julijana Gjorgjieva[a,d,1]

[a]Computation in Neural Circuits Group, Max Planck Institute for Brain Research, 60438 Frankfurt, Germany; [b]Department of Biology, Brandeis University, Waltham, MA 02454; [c]Department of Biology, Washington University in St. Louis, St. Louis, MO 63130; and [d]School of Life Sciences, Technical University of Munich, 85354 Freising, Germany

Edited by Terrence J. Sejnowski, Salk Institute for Biological Studies, La Jolla, CA, and approved August 04, 2020 (received for review October 20, 2019)

Homeostasis is indispensable to counteract the destabilizing effects of Hebbian plasticity. Although it is commonly assumed that homeostasis modulates synaptic strength, membrane excitability, and firing rates, its role at the neural circuit and network level is unknown. Here, we identify changes in higher-order network properties of freely behaving rodents during prolonged visual deprivation. Strikingly, our data reveal that functional pairwise correlations and their structure are subject to homeostatic regulation. Using a computational model, we demonstrate that the interplay of different plasticity and homeostatic mechanisms can capture the initial drop and delayed recovery of firing rates and correlations observed experimentally. Moreover, our model indicates that synaptic scaling is crucial for the recovery of correlations and network structure, while intrinsic plasticity is essential for the rebound of firing rates, suggesting that synaptic scaling and intrinsic plasticity can serve distinct functions in homeostatically regulating network dynamics.

homeostasis | cortical circuits | functional correlation | synaptic scaling | intrinsic plasticity

Neural circuits are faced with a fundamental problem: how to allow experience to alter and refine network connectivity during learning and experience-dependent plasticity, while still maintaining stability of function. Generating a neural system that is both stable and flexible is a nontrivial challenge and requires a prolonged period of development when multiple mechanisms at the level of single neurons and networks of neurons interact. Two powerful and fundamentally different forms of plasticity involved in this process are Hebbian mechanisms, which alter synaptic connectivity in a synapse-specific manner, and homeostatic mechanisms that maintain stable function by globally adjusting overall synaptic weights and neuronal excitability.

The development and refinement of visual response properties in the primary visual cortex (V1) involves classic synapse-specific mechanisms implementing the bidirectional form of Hebbian plasticity, such as long-term potentiation (LTP) and long-term depression (LTD), considered to be the cellular substrate for learning and memory (1). Associative Hebbian plasticity, however, drives positive feedback processes that lead to unstable network dynamics, and some form of homeostasis is needed to compensate for this inherent instability (2, 3). A large body of evidence shows that various homeostatic plasticity mechanisms, including synaptic scaling and intrinsic plasticity (4, 5), operate in the brain to maintain stability despite various internal and external perturbations. More specifically, homeostatic plasticity can elevate neural activity in response to sensory deprivation (6, 7) and suppress activity under conditions of overexcitation (8, 9).

Despite great efforts to describe homeostatic mechanisms at the single cell level, how network properties are homeostatically regulated is largely unknown. While Hebbian and homeostatic mechanisms operate at different timescales and can be induced by distinct cues (10–13), how they interact within complex, highly recurrent microcircuits, as those found in the cortex, to refine and maintain circuit function has remained elusive. A critical challenge has been the lack of detailed measurements of individual synaptic strengths and their potential impact on large-scale network dynamics, especially in a highly recurrent network like the cortex.

Here, we investigate two main questions. First, which aspects of network function are under homeostatic control? Second, why are there so many homeostatic mechanisms, and do they serve redundant or unique functions? To address these questions, we combine analysis of in vivo electrophysiological data during sensory deprivation in the rodent visual cortex and computational modeling of cortical synaptic plasticity and network dynamics. First, we analyzed the collective activity of multiple neurons in the monocular region of the primary visual cortex (V1m) during a classic monocular deprivation (MD) paradigm (lid suture) in freely behaving rats over 9 d during the critical period (14). Earlier work demonstrated that MD induces an initial drop in firing followed by the rates' homeostatic recovery despite long-lasting deprivation (14). Here, we reanalyzed these datasets to characterize the temporal evolution of higher-order network properties over the same 9-d period. Individual pairwise correlations, including correlation structure, weakened during brief MD but recovered during prolonged MD. Second, to understand how the cortical network exploits diverse homeostatic mechanisms to return firing rates and correlations to baseline (BL) after prolonged MD, we took advantage of a plastic spiking recurrent network model equipped with known plasticity and homeostatic mechanisms. Our work suggests that synaptic scaling is crucial

Significance

Despite decades of intense studies on homeostasis, network properties undergoing homeostatic regulation remain elusive. Furthermore, whether diverse forms of homeostatic plasticity are simply redundant or serve distinct functions is unclear. Here, our data show that functional correlations are subject to homeostatic regulation, both in terms of average amplitude and their structure. A computational model demonstrates that synaptic scaling is essential for the restoration of correlations and network structure, whereas intrinsic plasticity is crucial for the recovery of firing rates after perturbations, suggesting that synaptic scaling and intrinsic plasticity distinctly contribute to homeostatic regulation.

Author contributions: Y.K.W. and J.G. designed research; Y.K.W. performed research; Y.K.W., K.B.H., and J.G. contributed new reagents/analytic tools; Y.K.W. and J.G. analyzed data; Y.K.W. and J.G. wrote the paper; K.B.H. and G.G.T. provided experimental data; and G.G.T. provided input during writing of the paper.

The authors declare no competing interest.

This article is a PNAS Direct Submission.

[1]To whom correspondence may be addressed. Email: turrigiano@brandeis.edu or gjorgjieva@brain.mpg.de.

This article contains supporting information online at https://www.pnas.org/lookup/suppl/doi:10.1073/pnas.1918368117/-/DCSupplemental.

First published September 11, 2020.

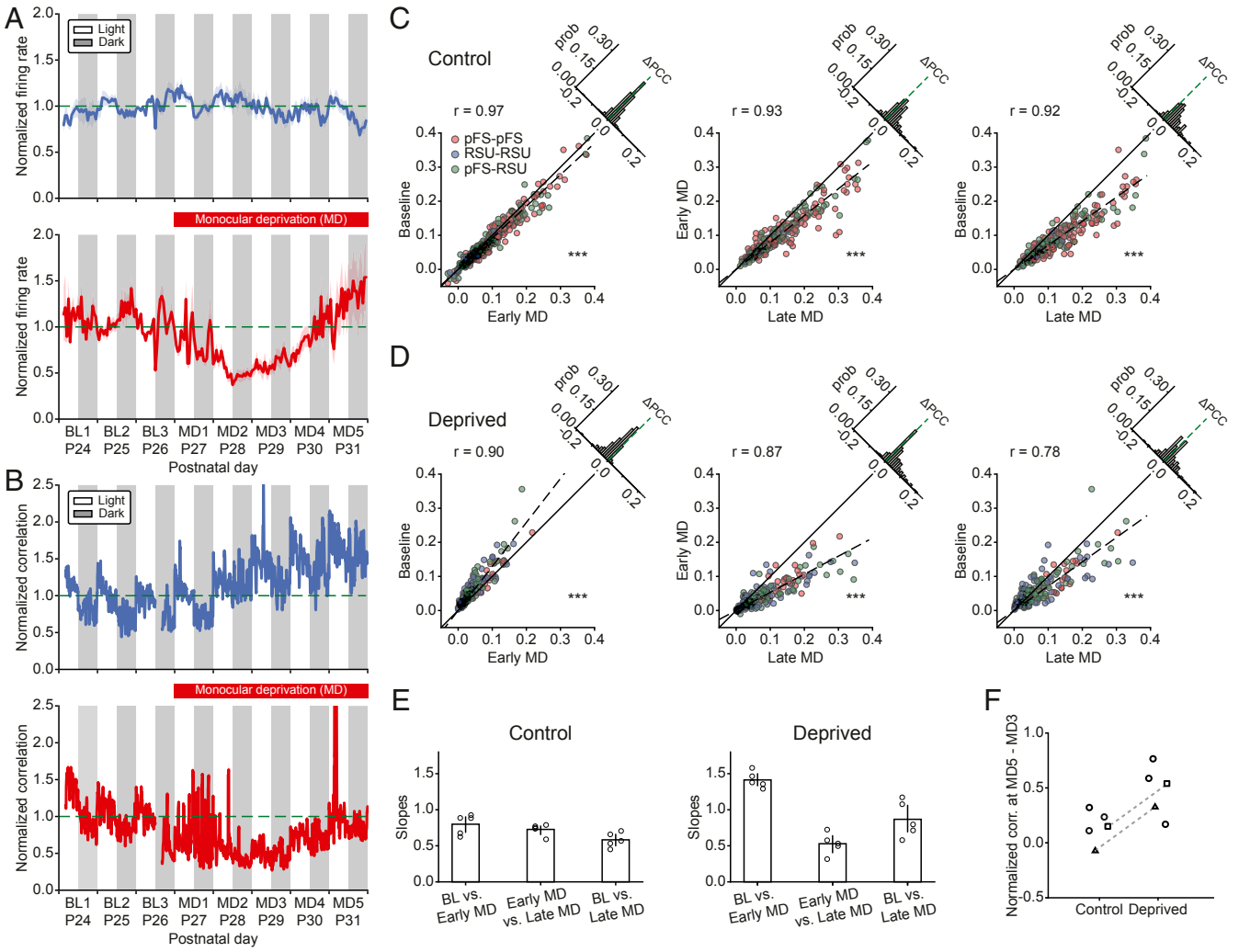

Fig. 1. MD induces an initial drop in correlations followed by their homeostatic recovery. (*A*) The average firing rates of 80 neurons from 5 control hemispheres (*Top*) and 104 neurons from 5 deprived hemispheres (*Bottom*) normalized to the firing rates at P26 in the light (horizontal dashed line). (*B*) The average pairwise correlations of 970 pairs from 5 control hemispheres (*Top*) and 2,455 pairs from 5 deprived hemispheres (*Bottom*) normalized to the correlations at P26 in the light (horizontal dashed line). (*C*) Correlation comparisons between BL and early MD (*Left*), between early MD and late MD (*Middle*), and between BL and late MD (*Right*) at the single cell-pair level of one control hemisphere. Different colors represent the correlations between different neuron types. Dashed lines are fitted regression lines crossing the origin. Upper left histograms indicate the distributions of correlation differences. ***$P < 0.001$ (Wilcoxon signed-rank test). (*D*) Same as *C* but for one deprived hemisphere. Here, for two hemispheres, we used MD3, and for the other three hemispheres, we used MD2, as early MD because different animals showed the biggest drop in correlations at different times. ***$P < 0.001$ (Wilcoxon signed-rank test). (*E*) Slopes of fitted regression lines for the correlation comparisons as in *C* and *D* for five control and five deprived hemispheres. (*F*) Change in the average normalized correlations between MD3 and MD5. Each data point denotes one hemisphere. Hemispheres from the same animals are marked with square or triangle symbols and connected by a dashed line. Data are shown as means ± SEM.

for the recovery of correlations and network structure, whereas intrinsic plasticity is essential for the rebound of firing rates. These results indicate that different homeostatic mechanisms act in the brain to independently regulate distinct network features.

Results

Pairwise Correlations during the Critical Period and in Response to MD. We first confirmed previous analysis of individual neurons recorded in vivo in the primary visual cortex during the critical period of plasticity (postnatal day [P]24 to P32). In these experiments, MD was performed after 3 d of BL activity and continued for the rest of the recordings. While firing rates of individual neurons remained relatively stable during normal development (Fig. 1*A*, *Top*), brief 2-d MD caused the firing rates to decrease to 40% of their BL values (Fig. 1*A*, *Bottom*) (6, 14). However, despite prolonged MD, over the next 3 to 4 d, firing rates gradually recovered to BL after an initial overshoot (Fig. 1*A*, *Bottom*) (6, 14). These effects were not only observed at the population level but also at the level of individual neurons (14). Here, we investigated higher-order network properties during normal development and following prolonged MD by calculating the next statistical moment beyond the firing rates, namely the pairwise spiking correlations between different neuron types (*Methods*). Specifically, we quantified the temporal evolution of the correlation coefficient of individual neuron pairs and of the average correlations across all pairs both during normal development and after perturbing visual input through MD. In control hemispheres, correlations, unlike firing rates, increased slightly as a function of age ($n = 5$ animals; Fig. 1*B*, *Top*). By contrast, in deprived hemispheres, correlations initially dropped over the first 2 d and then gradually rebounded to predeprivation levels ($n = 5$ animals; Fig. 1*B*, *Bottom*), displaying a similar pattern as the firing rates (Fig. 1*A*). As previously reported, we observed light–dark oscillations in the correlation

amplitudes, with higher correlations in the light and lower correlations in the dark (15).

To assess the degree to which correlations of individual neuron pairs changed beyond the population level, we evaluated single cell-pair correlations on different days. As in the earlier analysis, neurons were separated into putative parvalbumin-positive (PV^+) fast-spiking units (pFS) or regular-spiking units (RSUs) based on waveform and spiking characteristics (6, 14). Specifically, we focused on three different 12-h periods recorded in the light: 1) BL corresponding to P26; 2) a period that we called "early MD" when the largest drop of firing rates and correlations occurred, typically 2 or 3 d after BL (i.e., P28 or P29); and 3) a period that we called "late MD" corresponding to the time when the firing rates and correlations nearly recovered to BL (i.e., P31). As observed already for the average correlations, when combining all neuron pairs and animals, single cell-pair correlations increased during normal development covering the 6-d period during which recordings were performed. The increase between BL and early MD was small ($n = 435$ pairs; Fig. 1*C*, *Left*) ($r = 0.97$; $P < 10^{-21}$ [Wilcoxon signed-rank test]). Correlations at late MD were significantly greater than at early MD ($n = 253$ pairs; Fig. 1*C*, *Middle*) ($r = 0.93$; $P < 10^{-28}$ [Wilcoxon signed-rank test]). The developmental increase in correlations during the critical period became most obvious when we compared BL versus late MD ($n = 253$ pairs; Fig. 1*C*, *Right*) ($r = 0.92$; $P < 10^{-37}$ [Wilcoxon signed-rank test]). We did not observe any obvious differences in correlations among different cell types in that they all showed similar patterns of temporal evolution. Moreover, almost all neuronal pairs in a control hemisphere demonstrated an increase in correlation (Fig. 1*C*, *Right*).

Conversely, in deprived hemispheres, correlations of the majority of individual cell pairs, independent of their type, underwent a significant drop during early MD ($n = 190$ pairs; Fig. 1*D*, *Left*) ($r = 0.90$; $P < 10^{-24}$ [Wilcoxon signed-rank test]), followed by an increase during late MD ($n = 231$ pairs; Fig. 1*D*, *Middle*) ($r = 0.87$; $P < 10^{-27}$ [Wilcoxon signed-rank test]). The correlations during late MD recovered to a higher level than BL ($n = 190$ pairs; Fig. 1*D*, *Right*) ($r = 0.78$; $P < 10^{-4}$ [Wilcoxon signed-rank test]). We summarized the gradual increase of correlations in control hemispheres and the drop followed by recovery in deprived hemispheres by the slopes of the fitted regression lines of the individual pair data for each animal (Fig. 1*E*). Remarkably, despite a degree of variability across animals, the drop and recovery of correlations induced by MD were ubiquitous (*SI Appendix*, Fig. S1).

There are several possible mechanisms for the recovery of correlations during late MD in deprived hemispheres. First, it is possible that the correlations in the cortex simply follow the firing rates (16), which are homeostatically regulated. However, this scenario assumes a feedforward framework of signal transmission in which input correlations are fixed. In our experiments, input correlations under conditions of normal vision consist of a combination of signal and noise correlations. Closure of the eye during MD destroys signal correlations, thus decreasing overall input correlations, even though thalamic firing rates do not change during MD (17). Therefore, the only source of input correlations during prolonged MD is noise correlations. Under normal vision, cortical correlations in the dark (driven by noise input correlations) are approximately two-thirds of the correlations in the light (driven by intact signal input correlations) (15) (Fig. 1*B*). Combining these two results supports the conclusion that the homeostatic recovery of firing rates cannot explain the full recovery of cortical correlations and that network mechanisms are likely involved.

A second possibility suggests that the increase of correlations in deprived hemispheres could arise from the same underlying, possibly developmental, mechanism as in control hemispheres. To investigate this, we compared the increase in the average correlations between early MD, when the largest drop in the correlations occurs, and late MD, when the correlations have mostly recovered. We found that the increase of correlations in deprived hemispheres was consistently higher than in control hemispheres (Fig. 1*F*). This suggests that the increase of correlations in deprived hemispheres does not only have a developmental, age-dependent component but also a homeostatic recovery component in response to prolonged MD. We further found that the correlation changes between two adjacent 12-h light periods, as quantified by the slopes of the fitted regression lines, were different in the deprived from the control hemisphere in the same animals (*SI Appendix*, Fig. S2). This indicates that the increase in correlations between P29 and P31, the period corresponding to late MD, follows different temporal dynamics in control and deprived hemispheres.

Taken together, our results demonstrate an increase of correlations in deprived hemispheres during prolonged MD that is larger than the developmental increase of correlations in control hemispheres during normal development. Excluding other mechanisms such as coregulation with firing rates and age dependence, we propose that the recovery of correlations in deprived hemispheres during prolonged MD is due to homeostatic mechanisms, which are well known to operate in response to such perturbations (4, 5).

Network Structure after MD. While correlations at the single cell-pair level recovered during late MD, the difference between correlations at late MD and BL (Fig. 1*D*, *Right*) raised the possibility that the recovered network might have a different structure after recovery. To examine the evolution of network structure during normal development over the critical period and during prolonged MD, we examined the correlation matrices on different days. An example experiment shows that in the control hemisphere, the structure of the correlation matrix remained consistent over time ($n = 11$ neurons; Fig. 2*A*), whereas in the deprived hemisphere, the correlation structure initially weakened and recovered to a similar structure as BL ($n = 14$ neurons; Fig. 2*B*). MD induced heterogeneous changes in correlation structure across animals, despite an overall initial decrease and subsequent recovery (*SI Appendix*, Fig. S3). To quantify the similarity between the structure of correlation matrices at distinct time points, we calculated the $L1$ distance between correlations (*Methods*), which measures the absolute difference between them. Combining multiple animals revealed that in both control and deprived hemispheres, the correlation matrix at BL is more similar to the correlation matrix at early MD relative to randomly shuffling the latter for control ($n = 609$ pairs; Fig. 2*C*, *Left*) ($P < 10^{-58}$ [Wilcoxon signed-rank test]) and deprived hemispheres ($n = 505$ pairs; Fig. 2*D*, *Left*) ($P < 10^{-33}$ [Wilcoxon signed-rank test]). Additionally, the correlation structures at BL and late MD are more similar than chance level for control ($n = 609$ pairs; Fig. 2*C*, *Right*) ($P < 10^{-28}$ [Wilcoxon signed-rank test]) and deprived hemispheres ($n = 505$ pairs; Fig. 2*D*, *Right*) ($P < 10^{-30}$ [Wilcoxon signed-rank test]). These results suggest that despite a decrease in the correlation amplitude during early MD, the correlation structure is maintained throughout MD; hence, the network does not reorganize as correlations recover during late MD. In line with this finding, we found that the distance between BL and early MD in deprived hemispheres was not significantly different from that between BL and late MD ($n = 505$ pairs; Fig. 2*D*) ($P = 0.771$ [Wilcoxon signed-rank test]). However, for control hemispheres, the distance between BL and late MD was significantly higher than that between BL and early MD ($n = 609$ pairs; Fig. 2*C*) ($P < 10^{-46}$ [Wilcoxon signed-rank test]), due to the large increase in correlation amplitude during development (Fig. 1*C*). Interestingly, the correlation matrices

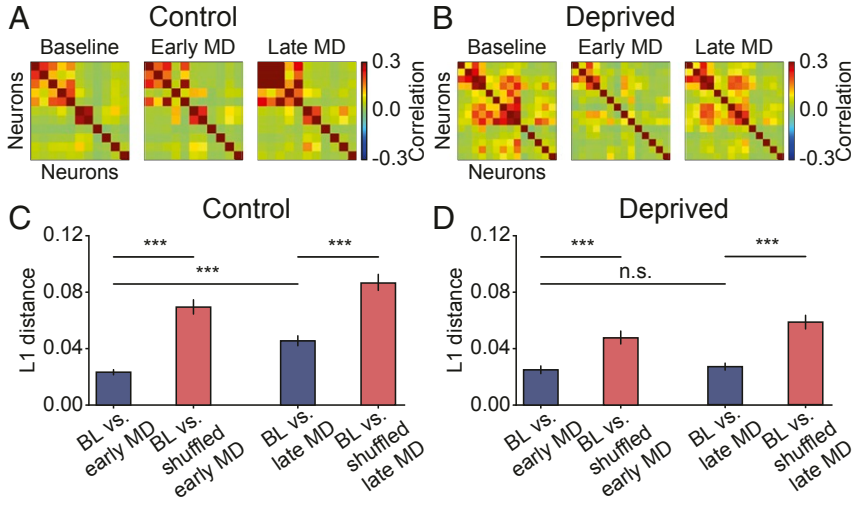

Fig. 2. Structure of correlation matrices is maintained after recovery. (*A*) Example correlation matrix of 11 neurons from 1 control hemisphere at 3 different time points. (*B*) Same as *A* but of 14 neurons from 1 deprived hemisphere. (*C*) *L*1 distance between correlations at BL and early MD, and at BL and late MD, vs. shuffled data for control hemispheres. (*D*) Same as *C* for deprived hemispheres. Data are shown as means ± SEM. ***$P < 0.001$; n.s., not significant ($P > 0.05$) (Wilcoxon signed-rank test).

are composed of several assemblies—groups of neurons exhibiting strong pairwise correlations (Fig. 2 *A* and *B*)—reminiscent of the clustered network structure reported in previous studies (18–21).

In conclusion, our analysis of V1 cortical activity recorded in vivo demonstrates that the pairwise correlations, in amplitude and structure, of these networks are homeostatically regulated following prolonged perturbation of normal sensory experience.

Formation of Structured Connectivity Assemblies during Training in a Recurrent Network Model. We next asked what mechanisms underlie the observed neuronal- and network-level changes during normal development and following a perturbation like MD. To understand how neural circuits exploit various synaptic plasticity and homeostatic mechanisms to first decrease and then recover both firing rates and correlations during MD, we built a plastic recurrent network model consisting of randomly connected excitatory and inhibitory spiking neurons (*Methods*). Model neurons received thalamic inputs, with thalamocortical synaptic efficacy onto inhibitory neurons set higher than onto excitatory neurons, consistent with previous experimental studies (22–24). Neuronal and network parameters were chosen to generate in vivo-like firing rates, with excitatory neurons firing at 5 Hz and inhibitory neurons firing at 13 Hz (6).

To generate the experimentally observed clustered correlation structure (Fig. 2 *A* and *B*), we included several experimentally characterized plasticity mechanisms (25) (*Methods*). We first tasked the network with the imprinting of connectivity assemblies starting from an initially random connectivity (Fig. 3*A*, *Left*). In contrast to previous models that used random, uncorrelated Poisson inputs (25) and in line with our observation that the networks show stronger pairwise correlations in the light than in the dark (15), we postulated that input correlations—as would be generated during natural vision—matter for the generation of clustered connections. Therefore, we trained the recurrent network by stimulating excitatory neurons with thalamocortical Poisson spiking inputs that had identical firing rates but differed in their correlation structures. For the training, excitatory neurons were randomly grouped into four identical assemblies, thereby simplifying network structure despite known heterogeneities in the data (*SI Appendix*, Fig. S3).

Before training with correlated inputs, the initial synaptic connections in the entire network were weak and identical between any pair of neurons of the same type (Fig. 3*A*, *Left*), resulting in asynchronous irregular network activity (Fig. 3*A*, *Middle*) and low correlations without clustered structure (Fig. 3*A*, *Right*). During training, excitatory neurons within a targeted assembly

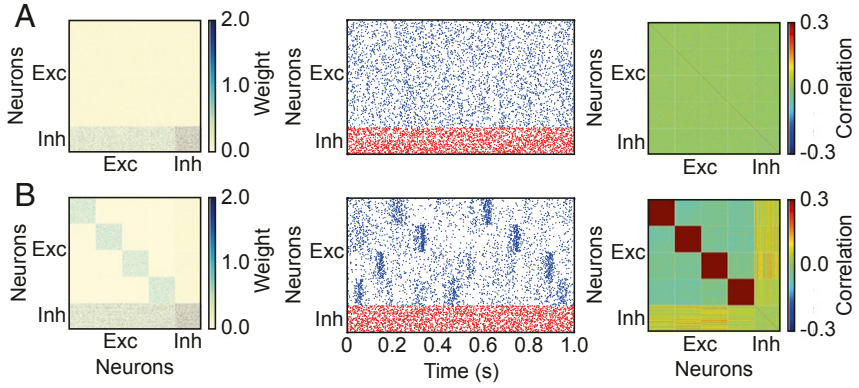

Fig. 3. Imprinting-connectivity assemblies with correlated inputs. (*A*) Before training: connectivity matrix (*Left*), spontaneous activity of excitatory (blue) and inhibitory (red) neurons (*Middle*), and correlation matrix (*Right*). (*B*) Same as *A* but after training.

received correlated inputs (*Methods*), which strengthened connectivity between them through Hebbian plasticity. After training, the excitatory subnetwork became structured with stronger synaptic connections between excitatory neurons within assemblies, while inhibitory neurons remained unstructured whereby inhibition is global and nonspecifically connects to all excitatory neurons (Fig. 3*B*, *Left*). As a result of this structure, the network no longer exhibited asynchronous irregular activity but rather blocks of activity in the excitatory neurons defined as occasional periods of high firing rate (Fig. 3*B*, *Middle*). The structured connectivity and block activity selectively generated high correlations between excitatory neurons within assemblies (Fig. 3*B*, *Right*).

A Model with Persistent Hebbian LTD and Homeostatic Plasticity Cannot Recover Correlations after MD. Using the structured model network as a baseline following normal cortical development after eye opening, we next wanted to investigate how this network responds to a sensory perturbation resembling MD. To achieve this, we needed to know how the inputs to the network are modified during MD. Previous experimental studies have reported that MD induces no change in the average firing rates of LGN, the visual area of the thalamus (17). Therefore, to simulate MD in our model network, we kept the firing rates of LGN inputs identical to that at BL but assumed that eye closure during MD considerably diminished input correlations. In the model, the excitatory neurons received uncorrelated Poisson inputs to denote the start of MD (Fig. 4*A*).

In addition to these changes in input correlations, recent experiments have revealed that brief MD (2 d) induces LTD at thalamocortical synapses onto excitatory and inhibitory neurons, with thalamocortical synapses onto inhibitory neurons depressing more than synapses onto excitatory neurons (24). The process of LTD is not instantaneous, so we assumed that synaptic connections from the thalamus to excitatory and inhibitory neurons undergo a linear decrease during the first 2 d of MD. To match experimental findings, the decrease in thalamocortical connections onto inhibitory neurons was larger (Fig. 4*A* and *Methods*). It is currently unknown when during MD this thalamocortical depression saturates, but since deprived-eye responsiveness reaches its minimum 2 to 3 d after the onset of MD (26), we assumed that the feedforward connections did not further decrease after this point, while keeping the inputs uncorrelated for the entire MD (Fig. 4*A*).

How does the recurrent network respond to these changes in input correlation structure and depression of feedforward connectivity strength that occur following MD? Although there are potentially multiple ways to achieve network stability and regulate network function, there are two fundamentally different mechanisms that have been well characterized experimentally: homeostatic adjustment of synaptic strengths and of intrinsic excitability (3, 27, 28). Excitatory neurons can regulate their activity by scaling incoming synaptic strengths in response to perturbations—a process known as synaptic scaling (4). This scaling is bidirectional in that it can increase and decrease synaptic strengths; it is global and operates in a multiplicative manner. In addition to synaptic scaling, neurons can alter the number of different ion channels to adjust intrinsic excitability, and consequently modify their firing thresholds, in response to perturbations (5, 13, 29).

Based on these experimental findings, in addition to Hebbian plasticity during training, we modeled these two distinct homeostatic mechanisms following MD: 1) synaptic scaling, which acts only on excitatory synapses (4, 6); and 2) intrinsic plasticity, which modifies the intrinsic excitability of both excitatory and inhibitory neurons (29, 30) (*Methods*). In the presence of persistent thalamocortical LTD, as during training, and both homeostatic mechanisms, the average firing rates of excitatory

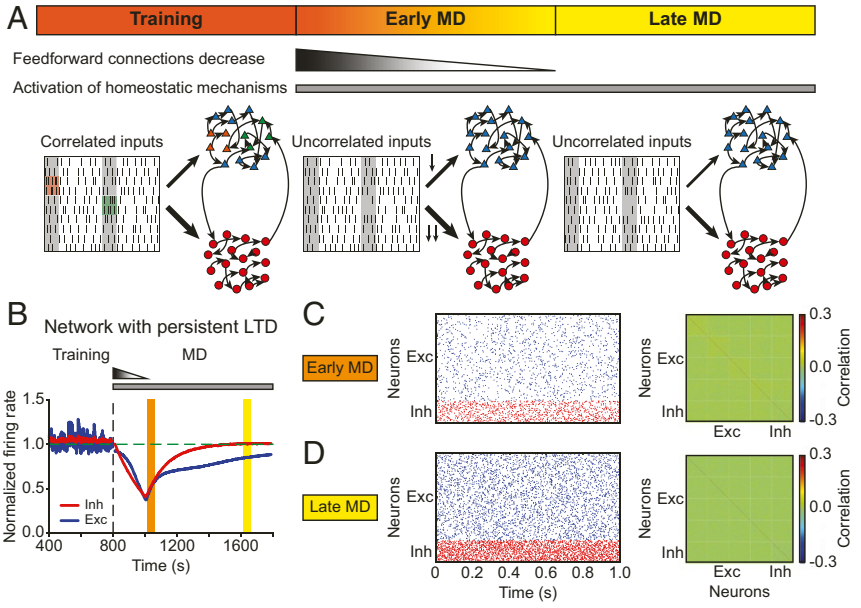

Fig. 4. The model with persistent Hebbian LTD and homeostatic plasticity fails to recover correlations. (*A*) Schematic description of the modeling framework during MD. The network consists of 80% excitatory neurons (triangles) and 20% inhibitory neurons (circles). Both of them receive thalamic inputs, and thalamocortical connections onto inhibitory neurons are stronger than onto excitatory neurons. Neurons receive correlated input during training at BL (*Left*) but uncorrelated input during early MD (*Middle*) and late MD (*Right*). During early MD, thalamocortical connections onto both excitatory and inhibitory neurons are depressed following a linear function in time, with thalamocortical connections onto inhibitory neurons depressed more strongly. The connections remain fixed during late MD. (*B*) The average normalized firing rates of excitatory (blue) and inhibitory (red) neurons. The vertical dashed line indicates the onset of MD. The horizontal dashed line indicates a normalized firing rate of 1.0. (*C*, *Left*) Spontaneous activity of excitatory (blue) and inhibitory (red) neurons during early MD. (*C*, *Right*) Correlation matrix during early MD indicated by the orange region in *B*. (*D*) Same as *C* but during late MD indicated by the yellow region in *B*.

and inhibitory neurons in the model network first decreased to 40% of BL, because slow homeostatic mechanisms could not overcome the feedforward synaptic depression and input decorrelation to recover firing rates. At the time that feedforward LTD saturated, firing rates started to increase due to homeostatic plasticity, resembling the recovery to BL observed experimentally during late MD (Fig. 4*B*; compare with Fig. 1*A*, *Bottom*).

Next, we investigated the evolution of higher-order aspects of network dynamics. Similar to the analysis of our data, we focused on two key time points after MD onset in the model: early MD, corresponding to the largest drop of firing rates (Fig. 4*B*, orange); and late MD, corresponding to the time when the firing rates recovered close to BL (Fig. 4*B*, yellow). The network showed irregular spiking dynamics with different firing rates during these two periods (Fig. 4 *C* and *D*, *Left*). The correlations between excitatory neurons first decreased during the period modeling early MD, as observed experimentally (Fig. 4*C*, *Right*; compare with Fig. 2*B*, *Middle*), but did not recover during the period corresponding to late MD (Fig. 4*D*, *Right*; compare with Fig. 2*B*, *Right*). We speculated that this failure to recover the correlations in the model network, despite the recovery of firing rates, could be the result of perturbing the structured connectivity between excitatory neurons within assemblies generated through training (Fig. 3*B*). Indeed, the average weights between excitatory neurons within an assembly depressed during the period corresponding to late MD (*SI Appendix*, Fig. S4).

To reveal the origin of this depression in the model network, we investigated the specific contribution of Hebbian plasticity and synaptic scaling to the average excitatory weight change within assemblies. Despite the overall potentiation of excitatory weights within assemblies induced by synaptic scaling during the period corresponding to early MD, continued LTD from Hebbian plasticity dominated over homeostatic plasticity, depressing all excitatory weights within assemblies and preventing the recovery of excitatory-to-excitatory correlations (*SI Appendix*, Fig. S5). In conclusion, this dominance of depression after MD prevents the recovery of structured connectivity, and consequently correlations, between excitatory neurons in a model with persistent Hebbian LTD despite homeostatic plasticity. This suggests that the relative timing and resulting competition between the two homeostatic mechanisms and ongoing Hebbian plasticity could be important for recovering different aspects of network dynamics.

The Attenuation of Hebbian LTD Together with Homeostatic Mechanisms Restores Firing Rates and Correlations during Prolonged MD. Previous work involving ocular dominance plasticity has shown that blocking Hebbian plasticity under normal rearing or after 6 d of MD does not cause any significant change in the response strength in the binocular region of V1, suggesting that the effects of Hebbian and homeostatic plasticity are negligible at each of the two steady states. These experiments also argued that the total effect of Hebbian plasticity in the deprived eye during the recovery phase is dominated by LTD but gradually approaches zero when homeostatic plasticity reaches its steady state (31). Motivated by these findings, we asked whether the recovery of excitatory correlations during the period corresponding to late MD in the model can be rescued by reducing the effect of Hebbian LTD. We proposed that the attenuation of Hebbian plasticity might occur through a metaplastic process where the amplitude of LTD dynamically adapts to the history of neuronal activity (*Methods*) (32, 33). Implementing metaplastic LTD preserved the recovery of average firing rates of both excitatory and inhibitory neurons (Fig. 5*A*). Similarly, the spiking rasters during the period corresponding to early MD showed asynchronous irregular activity (Fig. 5*B*, *Left*). In contrast to the model with persistent LTD, however, the metaplastic reduction in LTD enabled the return of structured excitatory activity during late MD (Fig. 5*C*, *Left*). Importantly, the excitatory correlation structure in the model during late MD homeostatically recovered after its initial dilution during early MD (Fig. 5*B* and Fig. 5*C*, *Right*; compare with Fig. 2*B*, *Middle* and *Right*). The decrease and recovery of correlations was the same across all neuron pairs within assemblies in our model because the trained assemblies were identical, unlike the heterogeneity in the data where the correlations of different neuron pairs

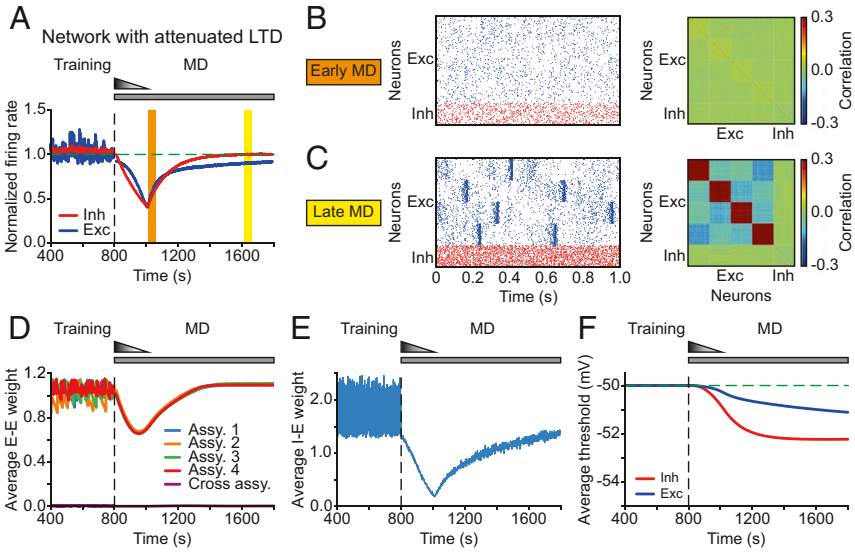

Fig. 5. The model with attenuated LTD recovers excitatory and inhibitory firing rates and excitatory correlations during MD. (*A*) The average normalized firing rates of excitatory (blue) and inhibitory (red) neurons. The vertical dashed line indicates the onset of MD. The horizontal dashed line indicates a normalized firing rate of 1.0. (*B*, *Left*) Spontaneous activity of excitatory (blue) and inhibitory (red) neurons during early MD. (*B*, *Right*) Correlation matrix during early MD indicated by the orange region in *A*. (*C*) Same as *B* but during late MD indicated by the yellow region in *A*. (*D*) Average excitatory-to-excitatory weights for each assembly and across assemblies. (*E*) Average inhibitory-to-excitatory weights that target all excitatory neurons independent of assembly membership. (*F*) Average firing thresholds of excitatory (blue) and inhibitory (red) neurons. The horizontal dashed line indicates the initial firing threshold.

underwent a varying degree of decrease and recovery (*SI Appendix*, Fig. S3). Adding heterogeneity to the model assemblies—for instance, by diversifying synaptic strengths, connectivity probabilities, or sizes—might be necessary to capture the diverse changes in correlation structures in the data. The metaplastic down-regulation of LTD in our model shifted the network from an LTD-dominant regime during early MD to an LTP/LTD-balanced regime during the recovery phase. Although this regime differs from previous studies in which the network remains in an LTD-dominant regime during most of the recovery phase (31), firing rates and correlations will recover provided that homeostatic plasticity greatly dominates over Hebbian LTD during the recovery phase.

We further investigated what other properties of the network changed as we modeled MD. Along with firing rates and excitatory correlations, the average excitatory weights within assemblies manifested the same pattern of drop and rebound (Fig. 5*D*), in contrast to the corresponding weights in the initial model with persistent LTD (*SI Appendix*, Fig. S4). Average inhibitory onto excitatory weights also decreased during early MD in the model (Fig. 5*E*), suggesting that the network reduced the amount of inhibition to elevate the decreased firing rates of excitatory neurons. During the period corresponding to late MD, overall inhibition increased to balance the gradually recovered excitation, keeping excitatory–inhibitory balance and avoiding winner-take-all dynamics where a single strongly connected assembly dominates the entire network (25). Furthermore, the average firing thresholds of excitatory and inhibitory neurons in the model network decreased as we modeled prolonged MD and reached a steady state as the firing rates approached their BL values (Fig. 5*F*).

Our experimental analysis revealed that, despite a decrease in the correlation amplitude during early MD, correlation structure is maintained throughout MD (Fig. 2*D*). Consistent with this, if network structure is completely erased during early MD in our model (as in the scenario without metaplastic LTD; Fig. 4), then homeostatic synaptic scaling during late MD cannot recover excitatory correlations because the backbone of recurrent circuitry from which to rebuild them has been lost. Otherwise, synaptic scaling can still rescue correlations even when the intensity or duration of LTD at thalamocortical synapses increases (*SI Appendix*, Fig. S6). In particular, we found that the intensity and duration of feedforward LTD have a different impact on the excitatory synaptic weights within assemblies, which shape excitatory correlation structure in the model. More intense and prolonged LTD causes a larger decrease in the firing rates, enabling the fast upscaling of excitatory synaptic weights within assemblies that recover correlations well before firing rates (*SI Appendix*, Fig. S6). Only prolonging feedforward LTD without affecting its intensity does not decrease firing rates as much (*SI Appendix*, Fig. S6), due to the lower firing thresholds of the neurons (*SI Appendix*, Fig. S7). The smaller drop in firing rates constrains the amount of synaptic upscaling, resulting in weaker excitatory correlation structure during the recovery phase. Consequently, network connectivity and correlations recover later than firing rates (*SI Appendix*, Fig. S6). These results suggest that correlation changes do not necessarily follow firing rate changes but are the product of interacting homeostatic mechanisms at the network level.

In summary, metaplastic regulation of LTD, together with synaptic scaling and intrinsic plasticity, is sufficient to capture both the recovery of excitatory and inhibitory firing rates and excitatory correlations during MD. Maintaining network structure during early MD is necessary for synaptic scaling to recover correlation structure during late MD. Hence, homeostatic modifications of overall synaptic weights and intrinsic excitability cooperate with Hebbian LTD to recover several aspects of network function following input perturbations.

Individual Homeostatic Mechanisms Have Different Functionality during MD. To determine the distinct contributions of the different homeostatic mechanisms for the recovery of firing rates and correlations during prolonged MD, we selectively eliminated each mechanism. When deactivating synaptic scaling during the entire period of MD in the model, we found that excitatory and inhibitory firing rates still recovered (Fig. 6*A*), whereas the excitatory correlations did not (Fig. 6*C*). Since synaptic scaling affects excitatory synaptic strengths, we hypothesized that the correlations failed to recover due to the inability of the network to recover its structured excitatory connectivity. Indeed, the average weights between excitatory neurons within assemblies remained low in the absence of synaptic scaling (*SI Appendix*, Fig. S8), eliminating structured block activity (Fig. 6*B*) and preventing the recovery of excitatory correlation structure during late MD (Fig. 6*C*). This suggests that synaptic scaling on excitatory synapses is indispensable for the recovery of excitatory correlations.

Similarly, without intrinsic plasticity during the entire MD period, neither excitatory nor inhibitory firing rates in the model recovered (Fig. 6*D*). This result was independent of the recovery of correlations. When the overall excitatory drive received by a single neuron within the same assembly was weak, low firing rates were accompanied by a poor degree of synchrony within assemblies (Fig. 6*E*), resulting in weak correlations (Fig. 6*F*). Increasing the overall excitation to a neuron, for instance, by increasing the connectivity probability within assemblies, could still generate structured block activity resulting in high correlations within assemblies but without recovering firing rates, especially for inhibitory neurons.

In conclusion, we demonstrated that two important forms of homeostatic plasticity, synaptic scaling and intrinsic homeostatic plasticity, are able to regulate distinct aspects of network activity.

Recovery of Inhibitory Correlations Requires Cotuning of Excitation and Inhibition. So far, we have focused on the recovery of excitatory and inhibitory firing rates through intrinsic plasticity and correlations between excitatory neurons through synaptic scaling on excitatory synapses. However, our results in Fig. 1 indicate that the other types of correlations that involve the inhibitory neurons undergo the same temporal profile during prolonged MD, with a drop during early MD and a recovery during late MD. Here, we investigated if the same homeostatic mechanisms identified above have different functionality during MD by minimally modifying our network architecture. In our network, the action of inhibition is global, where inhibitory neurons nonspecifically connect to all excitatory neurons. Hence, inhibitory neurons activate together with any excitatory assembly, resulting in weak excitatory–inhibitory and inhibitory–inhibitory correlations. Rather than considering global inhibition, we next modeled inhibition as cotuned with excitation where individual assemblies of inhibitory neurons connect exclusively to individual assemblies of excitatory neurons (*Methods*), inspired by recent experiments in the visual cortex (34). Due to this cotuning of inhibition with excitation, correlated structure emerged across all types of neurons. The excitatory–inhibitory and inhibitory–inhibitory correlations were high as the block activity generated by a given cortical excitatory assembly provides a major drive to inhibitory neurons (*SI Appendix*, Fig. S9).

Implementing the same protocol for inducing MD in our model, with depression of the feedforward weights and decorrelation of thalamocortical input, generated the same drop and recovery of firing rates and correlations, now involving both excitatory and inhibitory neurons (*SI Appendix*, Fig. S9). Notably, the same two forms of homeostatic plasticity, synaptic scaling and intrinsic homeostatic plasticity, successfully regulate distinct aspects of network activity also in these cotuned networks (*SI Appendix*, Fig. S10). Taken together, our result that homeostatic

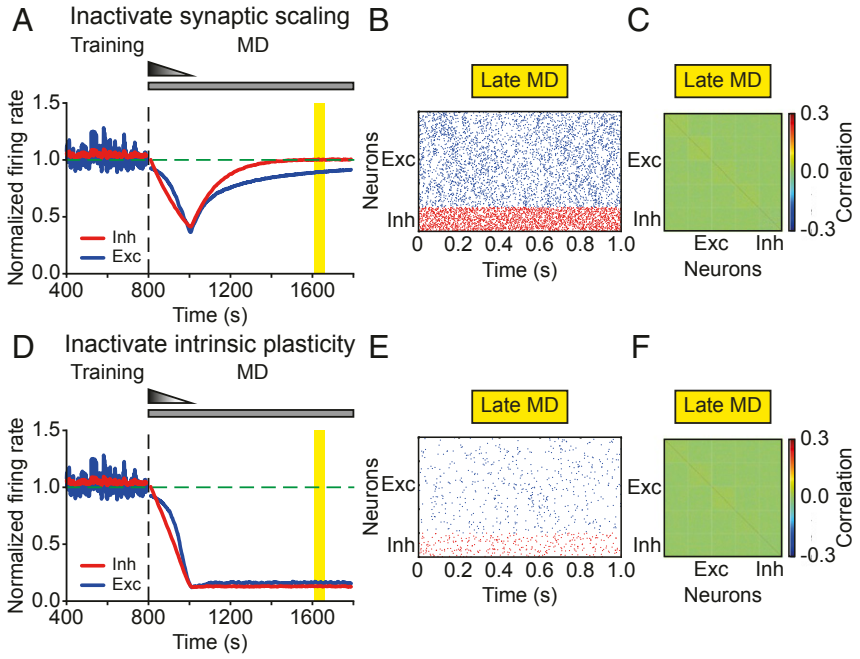

Fig. 6. Individual homeostatic mechanisms have different functionality during MD. (*A* and *D*) The average normalized firing rates of excitatory (blue) and inhibitory (red) neurons without synaptic scaling (*A*) or without intrinsic plasticity (*D*). The vertical dashed line indicates the onset of MD. The horizontal dashed line indicates a normalized firing rate of 1.0. (*B* and *E*) Spontaneous activity of excitatory (blue) and inhibitory (red) neurons during late MD without synaptic scaling (*B*) or without intrinsic plasticity (*E*). (*C* and *F*) Correlation matrix during late MD indicated by the yellow region in *A* and *D*, without synaptic scaling (*C*) or without intrinsic plasticity (*F*).

mechanisms regulate distinct aspects of cortical circuit dynamics applies also to different network architectures, suggesting that synaptic scaling and intrinsic plasticity quite generally influence different aspects of network function.

Discussion

A key question in the field of homeostatic plasticity is which aspects of neuronal activity are under homeostatic control. Recent studies have shown that, despite a high degree of synaptic plasticity during the critical period (35), firing rates of individual neurons remain remarkably constant during normal development (6) and when perturbed by sensory deprivation, rebound back to an individual set point despite continued deprivation (14). Here, we used in vivo data in rodent visual cortex to investigate whether higher-order cortical network properties are under homeostatic control. We found that—distinct from firing rates—correlations in control hemispheres increased slightly during early development. In contrast, correlations in deprived hemispheres initially decreased over the first 2–3 d and then gradually recovered to predeprivation levels, including in their structure. This recovery of correlations was independent of the recovery of firing rates and had a homeostatic component beyond the developmental increase of correlations. Modeling of this process revealed that this restoration of correlation structure could be accomplished through synaptic scaling, while firing rate homeostasis was dependent on intrinsic homeostatic plasticity. Together, these findings provide evidence that functional correlation structures are subject to homeostatic regulation.

Recovery of stimulus preference at the single cell level, as well as network correlation structure, has also been reported during repeated episodes of MD in the binocular region of visual cortex, each followed by eye reopening (36). However, in these ocular dominance plasticity studies, recovery occurring following eye reopening is TrkB-dependent and mediated by Hebbian LTP (37). This is mechanistically distinct from our work where recovery is governed by homeostatic mechanisms and where there is no competition between the closed and open eye.

Our modeling results suggest that the difference in the visual input from the thalamus at MD compared to BL does not seem to be important for cortical correlations. A proper experimental verification of this result would require the measurement of correlations in the thalamus during BL and during MD. Although these data are currently unavailable, there are data to indirectly verify this. Our analysis revealed that cortical correlations in deprived hemispheres recover to their BL level after 5 to 6 d of MD (Fig. 1*B*), regardless of possible correlation changes in the thalamus. In addition, we have previously shown that correlations in the dark are approximately two-thirds of the correlations in the light when the animals are in the awake behavioral state (15). These results suggest that correlated visual inputs only have a modest impact on the amplitude of cortical correlations, while recurrent connections might be the dominant contributor. Hence, following the elimination of visual input during MD, homeostatic mechanisms such as synaptic scaling can recover cortical correlations.

What might be the purpose of the recovered network correlations? Following lid suture to induce MD, the transmitted light through the closed eye lids is relatively weaker compared to the predeprivation condition. Therefore, we propose that the network's homeostatic recovery of correlations might be a way to amplify weak signals, promoting successful signal propagation to other cortical regions (38), which is essential for the animals' perception of the sensory environment (39). We predict that the recovery of correlation structure also has important functional implications for information transmission across cortical hierarchies. For instance, neurons in layer 2/3 process inputs from neurons in layer 4 and are highly influenced by its connectivity. If the recovered network in one layer undergoes a profound remodeling and ends up having a completely different correlation structure, adjustments in successive layers would be needed to keep the cortical network functional.

We cannot conclude from our data whether neurons with higher correlations are more strongly connected. However, as previously shown, functionally correlated neurons are more likely to be connected and more strongly if so (18, 19). We therefore assume that correlation strength is indicative of connection strength. In that sense, the identified clusters with strong correlations come from strongly connected assemblies consistent with previous experimental work (18, 19, 40). However, this is only the case for excitatory neurons (identified RSUs); since the number of sorted pFS cells was significantly lower than RSUs, we could not investigate their correlation structure.

To dissect the role of various homeostatic mechanisms to restore firing rates and correlations to BL despite prolonged MD, we built and analyzed a computational model with spiking neurons and biologically realistic plasticity rules. Upon training with correlated input patterns (41), imitating the BL condition in which animals receive normal visual inputs, the network exhibited structured spontaneous activity and developed stronger correlations within assemblies. Our model showed that decreasing thalamocortical connection strength (24) and decorrelating input patterns during MD degraded synaptic weights and decreased firing rates and correlations. This was accompanied by a depression in excitatory synaptic weights within assemblies and overall inhibitory synaptic weights in the model. Although experiments have not found significant changes in the strength of recurrent excitation within layer 4 (42), in layer 2/3, there is a general depression of excitatory input (28); a more systematic analysis that includes measurements within and across assemblies would be necessary to reveal selective depression of some connections.

Other modeling studies have investigated the interaction between Hebbian and homeostatic plasticity for the stable formation and maintenance of Hebbian assemblies in the context of memory storage and recall (43–45), which are different from the sensory deprivation paradigm studied here. Interestingly, a recent modeling framework for the homeostatic recovery from visual deprivation proposed that the disinhibitory effect of inhibitory plasticity, rather than synaptic scaling, can drive the recovery of firing rates and correlations in specific subnetworks of excitatory neurons (46), based on experimental results (40). We did not observe such specificity in our data, and inhibitory plasticity in our model was insufficient to recover either firing rates or correlations, necessitating instead intrinsic plasticity and synaptic scaling.

Our modeling results indicated that attenuating the depression effect of Hebbian plasticity was required to maintain clustered network structure during the process of recovery. This suggests that the effect of Hebbian plasticity becomes attenuated during prolonged MD, which then allows homeostatic plasticity to "catch up" and restore network properties. This is consistent with several experimental findings. For example, brief MD leads to occlusion of LTD in layer 4 in the primary visual cortex (24, 47), while homeostatic strengthening of CA1 synapses in the hippocampus is accompanied by a reduced ability of synapses to exhibit LTP (48). Furthermore, during MD, the effects of Hebbian plasticity, which is originally LTD-dominant, become negligible as homeostatic plasticity reaches its steady state (31).

Importantly, in the face of ongoing plasticity, we found that two different forms of homeostatic plasticity can serve distinct functions in recovering network function. First, intrinsic plasticity as a mechanism that affects individual neuron properties, such as the firing threshold, is essential for the rebound of firing rates. Since it does not act directly on the synaptic weights, it has no significant impact on the recovery of correlations. We implemented intrinsic plasticity by adjusting the firing threshold, which effectively shifts the neuronal input–output function to keep the model sufficiently general. Biophysically, intrinsic plasticity can be implemented by changes in the density and function of voltage-gated channels (5, 49, 50).

Unlike intrinsic plasticity, synaptic scaling regulates synaptic strengths directly and is crucial for the recovery of correlation and network structure in the model. Mechanistically, this regulation is fundamentally distinct from Hebbian plasticity. The regulating process involves an enhanced accumulation of α-amino-3-hydroxy-5-methyl-4-isoxazolepropionic acid (AMPA) receptor (AMPAR) in the postsynaptic membrane, which can be mediated by the proinflammatory cytokine tumor-necrosis factor-α (TNF-α) produced by glia (10), the immediate-early gene Arc (11), $\beta 3$ integrins (51), and other molecules. Crucially, the scaling is bidirectional, global, and operates in a multiplicative manner (4), although there is some evidence for dendritic branch-specific scaling in some neocortical cell types (52). During recovery, multiplicative scaling potentiates synaptic weights within assemblies more than across assemblies in our model, preserving the relative strength of synaptic inputs and enabling the recovery of correlation structure.

The distinct functional roles fulfilled by synaptic scaling and intrinsic plasticity apply in the context of the present constellation of plasticity rules. We found that synaptic scaling alone is insufficient to recover the firing rates in our model, especially inhibitory firing rates. The critical model assumption that derives this conclusion is that excitatory and inhibitory connections onto inhibitory neurons do not change during MD (*SI Appendix*, *Supplementary Text*). However, increasing synaptic strengths also boosts neuronal responses, which raises the possibility that synaptic scaling alone might be able to recover firing rates with a different combination of plasticity rules. One straightforward possibility to recover the firing rates of inhibitory neurons is either to increase the total excitation to inhibitory neurons, for example, by upscaling the excitatory-to-inhibitory connections, or to decrease the total inhibition to inhibitory neurons, for example, by downscaling the inhibitory-to-inhibitory connections. Interestingly, synaptic scaling onto inhibitory neurons was recently found to organize model recurrent networks around criticality, independently of firing rates (53). This suggests that homeostatic plasticity in excitatory elements might be important for the recovery of firing rates and correlations, while plasticity in inhibitory elements for the recovery of criticality. It still remains to be tested whether and how excitatory and inhibitory connections onto inhibitory neurons change in the context of homeostatic regulation in vivo. We highlight that including spiking neurons in our model and training the BL network with correlated inputs enabled us to study the emergence, dilution, and recovery of correlation structure during prolonged MD, which is not possible in the unstructured randomly connected networks studied in other models (53), even if firing rates recover. Furthermore, our implementation of Hebbian and homeostatic plasticity with appropriate biologically motivated timescales suggests a nontrivial cooperation between Hebbian and homeostatic plasticity, with the first being attenuated while the latter is in full operation.

In conclusion, our analysis reveals an important, previously unidentified network feature that is homeostatically regulated during perturbation of normal circuit dynamics in the visual cortex. The finding that not only the average correlations but also the correlation structure recover has interesting implications for the recovery of computations in these circuits that might be encoded in nonrandom connectivity patterns. Moreover, our network model with spiking neurons and experimentally characterized homeostatic mechanisms allowed us to dissect the role of each on different aspects of network dynamics, suggesting that different homeostatic mechanisms serve unique, rather than redundant, functions.

Table 1. Neuron model parameters

Symbol	Value	Unit	Description
U^{rest}	−70	mV	Resting membrane potential
U^{exc}	0	mV	Excitatory reversal potential
U^{inh}	−80	mV	Inhibitory reversal potential
τ^{ref}	5	ms	Duration of refractory period
τ^{m}_{exc}	20	ms	Membrane time constant of excitatory neurons
τ^{m}_{inh}	10	ms	Membrane time constant of inhibitory neurons
τ^{ampa}	5	ms	AMPA decay time constant
τ^{gaba}	10	ms	GABA decay time constant
τ^{nmda}	100	ms	NMDA decay time constant
α	0.5	-	Receptor weighting factor

-, no units.

Methods

Firing Rates. To obtain the normalized firing rate evolution for different animals, the firing rates of each animal were normalized to the average firing rate at P26 during the light period. Note that, here, the analysis of firing rates was restricted to MD5 because for the higher-order network feature analysis (the pairwise correlations), the number of available, continuously recorded cells beyond this period was insufficient. Therefore, although the firing rates still seem to be above BL at MD5—a trend identical to that reported in the previous study (14)—they eventually return to BL by MD6 (14).

Pairwise Correlations. Each spike train was binned into spike counts of bin size 100 ms, generating a vector of spike counts for each cell. The spike-count correlation coefficient ρ for a pair of neurons was computed in 30-min episodes using a sliding window of 5 min. We averaged these values for each pair every single half day (12 h), thus computing the correlation coefficient for light and dark conditions separately:

$$\rho_{X,Y} = \frac{\mathbf{E}[(X-\mu_X)(Y-\mu_Y)]}{\sigma_X \sigma_Y},$$

where X and Y represent the spike-count vectors of two cells, respectively; μ_X and μ_Y are the means of X and Y; σ_X and σ_Y denote the standard deviations of X and Y; $\mathbf{E}$ is the expectation. This produced the matrices of pairwise spike-count correlations on different half days. Just like the firing rates, to generate the normalized correlation curve across animals, the correlations of each animal were normalized to the average correlations at P26 during the light period.

The correlation matrices in Fig. 2 *A* and *B* were clustered using hierarchical clustering during BL, and the same neuron order was preserved at later time points.

Quantification of Changes in Correlation Structure. We first generated a shuffled matrix $\boldsymbol{A}'$ by redistributing the off-diagonal entries of the original matrix $\boldsymbol{A}$ while keeping the matrix $\boldsymbol{A}'$ symmetric. Then, we computed the absolute difference between the shuffled matrix $\boldsymbol{A}'$ and the correlation matrix at BL $\boldsymbol{B}$:

$$\boldsymbol{M} = |\boldsymbol{A}' - \boldsymbol{B}|.$$

The elements of the upper triangular part of $\boldsymbol{M}$ were used to form a vector of the absolute difference, known as the $L1$ distance, between correlations. Vectors from different animals were then concatenated into a single vector. During shuffling, only the elements corresponding to a given animal were shuffled, i.e., animal identity was preserved.

Neuron and Network Model. Single neurons were modeled as leaky integrate-and-fire with membrane potential of neuron i, U_i, given by (54):

$$\tau^{m}\frac{dU_i}{dt} = (U^{\text{rest}} - U_i) + g_i^{\text{ext}}(t)(U^{\text{exc}} - U_i) + g_i^{\text{inh}}(t)(U^{\text{inh}} - U_i),$$

where τ^m is the membrane time constant, and U^{rest} is the resting potential. The neuron elicited a spike when its membrane potential reached the spiking threshold U^{thr}. After a spike, the membrane potential was reset to U^{rest}. The neuron also had a refractory period τ^{ref} after a spike. Inhibitory neurons also followed the same integrate-and-fire formalism but with a shorter membrane time constant. The values of all neuron model parameters are listed in Table 1.

The network model consisted of 800 excitatory and 200 inhibitory leaky integrate-and-fire neurons, which were randomly connected with a probability of 20%. Excitatory neurons were randomly grouped into four nonoverlapping groups. Each excitatory and inhibitory neuron received external excitatory input from 1,000 neurons firing with Poisson statistics at an average firing rate of 5 Hz, with synaptic strength $J^{\text{ext}\to E}$ and $J^{\text{ext}\to I}$, respectively.

Excitatory synapses have a fast AMPA component and a slow *N*-methyl-D-aspartic acid (NMDA) component. Dynamics of excitatory conductances are given by:

$$\tau^{\text{ampa}}\frac{dg_i^{\text{ampa}}}{dt} = -g_i^{\text{ampa}} + \sum_{j\in\text{exc}} J_{ij}S_j(t),$$

$$\tau^{\text{nmda}}\frac{dg_i^{\text{nmda}}}{dt} = -g_i^{\text{nmda}} + g_i^{\text{ampa}},$$

$$g_i^{\text{exc}}(t) = \alpha g_i^{\text{ampa}}(t) + (1-\alpha)g_i^{\text{nmda}}(t).$$

Here, J_{ij} is the synaptic strength from neuron j to neuron i. If the connection does not exist, J_{ij} was set to 0. $S_j(t)$ is the spike train of neuron j, which is defined as $S_j(t) = \sum_k \delta(t - t_j^k)$, where δ is the Dirac delta function and t_j^k, the spikes times k of neuron j. α is a weighting parameter. Dynamics of inhibitory conductances are given by:

$$\tau^{\text{gaba}}\frac{dg_i^{\text{inh}}}{dt} = -g_i^{\text{inh}} + \sum_{j\in\text{inh}} J_{ij}S_j(t).$$

The values of all network parameters are listed in Table 2.

Training Procedure. We implemented the network in three stages: initialization stage, a training stage, and an MD stage. All plasticity except for excitatory-to-excitatory plasticity was present in the first 100 s of the simulation to initialize the network and obtain network activity before training.

Subsequently, the training process started. During training, correlated stimuli were presented sequentially to each assembly for 1 s, with 3-s gaps in between stimulus activations. While correlated stimuli were presented to 1 assembly, the remaining neurons received inputs from 1,000 independent neurons firing with Poisson statistics at an average firing rate of 5 Hz. The firing rate of the correlated inputs was also 5 Hz. Correlated inputs for the training were generated following previous studies (33, 55). Specifically, we used a copying probability of 0.4 from individual uncorrelated Poisson source trains and a copying probability of 0.6 from a common Poisson source, all with the same firing rates.

The weight matrix obtained after training was used to induce MD in the simulations. MD simulations started with 3 s without plasticity when inhibitory spike timing-dependent plasticity (iSTDP) was activated, while other plasticity and homeostatic mechanisms were activated at 10 s. At the same time, the feedforward connections onto excitatory and inhibitory neurons linearly decreased by 8 and 15% from 10 to 210 s and, afterward, were kept fixed.

Table 2. Network model parameters

Symbol	Value	Unit	Description
N_E	800	-	Number of excitatory neurons
N_I	200	-	Number of inhibitory neurons
p	0.2	-	Connectivity probability
J^{EE}	0.2	-	Initial E-to-E connection weight
J^{EI}	2.0	-	Initial I-to-E connection weight
J^{IE}	0.2	-	E-to-I connection weight
J^{II}	2.0	-	I-to-I connection weight
J^{EE}_{min}	0.0	-	Minimal E-to-E connection weight
J^{EE}_{max}	1.2	-	Maximal E-to-E connection weight
J^{EI}_{min}	0.0	-	Minimal I-to-E connection weight
J^{EI}_{max}	6.0	-	Maximal I-to-E connection weight
$J^{\text{ext}\to E}$	0.78	-	Initial external-to-E connection weight
$J^{\text{ext}\to I}$	0.85	-	Initial external-to-I connection weight

E, excitatory; I, inhibitory. -, no units.

Table 3. Plasticity model parameters

Symbol	Value	Unit	Description
r_0^E	5	Hz	Target firing rate of excitatory neurons
r_0^I	13	Hz	Target firing rate of inhibitory neurons
τ^+	16.8	ms	Time constant of presynaptic detector
τ^-	33.7	ms	Time constant of faster postsynaptic detector
τ^{slow}	114	ms	Time constant of slower postsynaptic detector
A^-	0.0071	-	Amplitude of LTD
A^+	0.0065	-	Amplitude of LTP
τ^{iSTDP}	0.02	s	Time constant of synaptic trace for iSTDP
η^{iSTDP}	1	-	Learning rate of iSTDP
τ^{est}	20	s	Time constant of firing rate estimator
τ^{ss}	200	s	Time constant of synaptic scaling
η^{ip}	0.00125	mV/s	Learning rate of intrinsic plasticity

-, no units.

Plasticity. To form the clustered correlation structure observed experimentally, we followed previous modeling studies (25) and modeled the plasticity of excitatory-to-excitatory synapses using triplet STDP (32) of inhibitory-to-excitatory synapses using iSTDP (56, 57) and also included heterosynaptic plasticity operating on excitatory-to-excitatory synapses.

The triplet STDP rule describes synaptic plasticity based on triplets of spikes and captures experiments where the rate of pre- and postsynaptic neurons varies (58). The triplet STDP rule enables the formation of bidirectional connections, a necessity for the formation of clustered architectures (41, 59). According to this rule, the synaptic strength from excitatory neuron j to excitatory neuron i follows:

$$\frac{dJ_{ij}^{EE}}{dt} = -z_i^-(t)A^- S_j(t) + z_j^+(t)A^+ z_i^{\text{slow}}(t-\epsilon)S_i(t).$$

Here, A^- and A^+ are the amplitude of the weight change induced by a post–pre pair or a post–pre–post triplet of spikes. ϵ is a small positive constant. The synaptic traces for neuron i (and similarly for neuron j) $z_i^+(t)$, $z_i^-(t)$, and $z_i^{\text{slow}}(t)$ evolve according to $\frac{dz_i^n}{dt} = -\frac{z_i^n}{\tau^n} + S_i(t)$ with different time constants τ^n, where $n = \{+, -, \text{slow}\}$.

According to iSTDP, the synaptic strength from inhibitory neuron j to excitatory neuron i follows:

$$\frac{dJ_{ij}^{EI}}{dt} = \eta^{\text{iSTDP}}(x_i - 2r_i^0\tau^{\text{iSTDP}})S_j(t) + \eta^{\text{iSTDP}}x_j S_i(t),$$

where x_i and x_j are the synaptic traces of the postsynaptic excitatory neuron i and presynaptic inhibitory neuron j, which are described by $\frac{dx_i}{dt} = -\frac{x_i}{\tau^{\text{iSTDP}}} + S_i(t)$, with r_i^0, τ^{iSTDP}, and η denoting the target firing rate of neuron i (and similarly for neuron j), the time constant of the synaptic trace and the learning rate of iSTDP, respectively.

Excitatory-to-inhibitory connections and inhibitory-to-inhibitory connections were nonplastic since their plasticity has been much less investigated experimentally and computationally. All plastic weights were subject to upper bounds.

Heterosynaptic plasticity. We also modeled normalization in the form of heterosynaptic plasticity, which ensures that the sum of all incoming excitatory synaptic weights at each postsynaptic excitatory neuron is kept below a target (60). This form of normalization has been found to be essential in maintaining clustered structures upon their formation (25). Hence, the synaptic strength from excitatory neuron j to excitatory neuron i was modified according to heterosynaptic plasticity as follows:

$$J_{ij}^{EE}(t) \leftarrow J_{ij}^{EE}(t) - \frac{1}{N_i^E}\left(\sum_j J_{ij}^{EE}(t) - \beta\sum_j J_{ij}^{EE}(0)\right),$$

where N_i^E is the number of nonzero elements. As heterosynaptic plasticity also imposed a constraint on the excitatory-to-excitatory synaptic weight, β was set to 1.08 so that J_{ij}^{EE} becomes approximately J_{max}^{EE}. Heterosynaptic plasticity was implemented every 1 s and only acting when the $\sum_j J_{ij}^{EE}(t)$ was larger than $\beta\sum_j J_{ij}^{EE}(0)$.

Metaplasticity. The amplitude of LTD for neuron i, A_i^-, follows:

$$A_i^- \leftarrow A_i^- \frac{x_i^{\text{est}}}{\tau^{\text{est}} r_i^0}.$$

Here, x_i^{est} denotes the firing-rate estimator defined as $\frac{dx_i^{\text{est}}}{dt} = -\frac{x_i^{\text{est}}}{\tau^{\text{est}}} + S_i(t)$, with τ^{est} being the integration time constant of x_i^{est}. If the firing rate of a neuron was close to its target, r_i^0, then $\frac{x_i^{\text{est}}}{\tau^{\text{est}} r_i^0} \approx 1$. Metaplasticity was implemented every 30 s. Furthermore, A_i^- was bounded below by 15% of its initial value to ensure that the effect of Hebbian plasticity eventually becomes negligible, as shown previously (31).

Homeostatic mechanisms: synaptic scaling and intrinsic plasticity. The evolution of synaptic strength from excitatory neuron j to excitatory neuron i via synaptic scaling is given by:

$$\tau^{ss}\frac{dJ_{ij}^{EE}}{dt} = J_{ij}^{EE}\left(1 - \frac{x_i^{\text{est}}}{\tau^{\text{est}} r_i^0}\right),$$

where τ^{ss} represents the time constant of synaptic scaling.

The firing threshold of neuron i regulated by intrinsic plasticity is given by:

$$\frac{dU_i^{\text{thr}}}{dt} = \eta^{ip}\left(\frac{x_i^{\text{est}}}{\tau^{\text{est}}} - r_i^0\right),$$

where η^{ip} is the learning rate of intrinsic plasticity. Initial firing threshold was set to -50 mV.

The values of all plasticity parameters are listed in Table 3.

Cotuned Network. The cotuned network model consisted of 800 excitatory and 200 inhibitory neurons. Excitatory and inhibitory neurons were divided into four nonoverlapping groups. The connectivity probability within the same groups is 20%. Inhibitory neurons exclusively connected with excitatory neurons in the same group. The simulations started with 3 s without plasticity when iSTDP was activated, while other plasticity and homeostatic mechanisms were inactivated for the first 210 s. After that, other plasticity and homeostatic mechanisms were activated. The feedforward connections onto excitatory and inhibitory neurons linearly decreased by 4 and 8% from 210 to 410 s. From 410 s onward, feedforward connections were kept fixed. For the sake of simplicity, we implemented metaplasticity differently from the original model. Instead of dynamically modifying the LTD amplitude, here, we disabled Hebbian plasticity at 410 s. Parameters used in cotuned network models, which are different from the original model, are listed in *SI Appendix*, Table S1.

Simulations. Data analysis and numerical simulations were performed in Python and Julia. All differential equations were implemented by Euler integration with a time step of 0.1 ms.

Data Availability. The code used for data analysis and model simulations is available at GitHub (https://github.com/comp-neural-circuits/homeostasis). The data is available at Figshare (https://figshare.com/projects/Homeostasis/80936).

ACKNOWLEDGMENTS. We thank all members of J.G.'s group for comments and discussions. This work was supported by the Max Planck Society (Y.K.W. and J.G.), NIH Grants R01 EY025613 and R35 NS111562 (to G.G.T.), and NIH Grant R00 NS089800 (to K.B.H.). This project has received funding from the European Research Council under European Union's Horizon 2020 Research and Innovation Program Grant 804824 (to J.G.).

1. G. B. Smith, A. J. Heynen, M. F. Bear, Bidirectional synaptic mechanisms of ocular dominance plasticity in visual cortex. *Philos. Trans. R. Soc. Lond. B Biol. Sci.* **364**, 357–367 (2008).
2. L. F. Abbott, S. B. Nelson, Synaptic plasticity: Taming the beast. *Nat. Neurosci.* **3** 1178–1183 (2000).
3. G. G. Turrigiano, S. B. Nelson, Homeostatic plasticity in the developing nervous system. *Nat. Rev. Neurosci.* **5**, 97–107 (2004).
4. G. G. Turrigiano, K. R. Leslie, N. S. Desai, L. C. Rutherford, S. B. Nelson, Activity-dependent scaling of quantal amplitude in neocortical neurons. *Nature* **391**, 892–896 (1998).
5. N. S. Desai, L. C. Rutherford, G. G. Turrigiano, Plasticity in the intrinsic excitability of cortical pyramidal neurons. *Nat. Neurosci.* **2**, 515–520 (1999).
6. K. B. Hengen, M. E. Lambo, SD. Van Hooser, D. B. Katz, G. G. Turrigiano, Firing rate homeostasis in visual cortex of freely behaving rodents. *Neuron* **80**, 335–342 (2013).

7. T. Keck *et al.*, Synaptic scaling and homeostatic plasticity in the mouse visual cortex in vivo. *Neuron* **80**, 327–334 (2013).
8. D. P. Seeburg, M. Feliu-Mojer, J. Gaiottino, D. T. Pak, M. Sheng, Critical role of cdk5 and polo-like kinase 2 in homeostatic synaptic plasticity during elevated activity. *Neuron* **58**, 571–583 (2008).
9. D. M. Evers *et al.*, Plk2 attachment to NSF induces homeostatic removal of GluA2 during chronic overexcitation. *Nat. Neurosci.* **13**, 1199–1207 (2010).
10. D. Stellwagen, R. C. Malenka, Synaptic scaling mediated by glial TNF-α. *Nature* **440**, 1054–1059 (2006).
11. J. D. Shepherd *et al.*, Arc/arg3.1 mediates homeostatic synaptic scaling of AMPA receptors. *Neuron* **52**, 475–484 (2006).
12. A. Joseph, G. G. Turrigiano, All for one but not one for all: Excitatory synaptic scaling and intrinsic excitability are coregulated by CaMKIV, whereas inhibitory synaptic scaling is under independent control. *J. Neurosci.* **37**, 6778–6785 (2017).
13. G. Daoudal, D. Debanne, Long-term plasticity of intrinsic excitability: Learning rules and mechanisms. *Learn. Mem.* **10**, 456–465 (2003).
14. K. B. Hengen, A. T. Pacheco, J. N. McGregor, S. D. Van Hooser, G. G. Turrigiano, Neuronal firing rate homeostasis is inhibited by sleep and promoted by wake. *Cell* **165**, 180–191 (2016).
15. A. T. Pacheco *et al.*, Rapid and active stabilization of visual cortical firing rates across light–dark transitions. *Proc. Natl. Acad. Sci. U.S.A.* **116**, 18068–18077 (2019).
16. J. De La Rocha, B. Doiron, E. Shea-Brown, K. Josić, A. Reyes, Correlation between neural spike trains increases with firing rate. *Nature* **448**, 802–806 (2007).
17. M. L. Linden, A. J. Heynen, R. H. Haslinger, M. F. Bear, Thalamic activity that drives visual cortical plasticity. *Nat. Neurosci.* **12**, 390–392 (2009).
18. H. Ko *et al.*, Functional specificity of local synaptic connections in neocortical networks. *Nature* **473**, 87–91 (2011).
19. L. Cossell *et al.*, Functional organization of excitatory synaptic strength in primary visual cortex. *Nature* **518**, 399–403 (2015).
20. R. Perin, T. K. Berger, H. Markram, A synaptic organizing principle for cortical neuronal groups. *Proc. Natl. Acad. Sci. U.S.A.* **108**, 5419–5424 (2011).
21. Y. Yoshimura, J. L. Dantzker, E. M. Callaway, Excitatory cortical neurons form fine-scale functional networks. *Nature* **433**, 868–873 (2005).
22. S. J. Cruikshank, T. J. Lewis, B. W. Connors, Synaptic basis for intense thalamocortical activation of feedforward inhibitory cells in neocortex. *Nat. Neurosci.* **10**, 462–468 (2007).
23. X.-Y. Ji *et al.*, Thalamocortical innervation pattern in mouse auditory and visual cortex: Laminar and cell-type specificity. *Cereb. Cortex* **26**, 2612–2625 (2015).
24. N. J. Miska, L. M. Richter, B. A. Cary, J. Gjorgjieva, G. G. Turrigiano, Sensory experience inversely regulates feedforward and feedback excitation-inhibition ratio in rodent visual cortex. *eLife* **7**, e38846 (2018).
25. A. Litwin-Kumar, B. Doiron, Formation and maintenance of neuronal assemblies through synaptic plasticity. *Nat. Commun.* **5**, 5319 (2014).
26. M. Y. Frenkel, M. F. Bear, How monocular deprivation shifts ocular dominance in visual cortex of young mice. *Neuron* **44**, 917–923 (2004).
27. G. Turrigiano, Too many cooks? Intrinsic and synaptic homeostatic mechanisms in cortical circuit refinement. *Annu. Rev. Neurosci.* **34**, 89–103 (2011).
28. M. E. Lambo, G. G. Turrigiano, Synaptic and intrinsic homeostatic mechanisms cooperate to increase L2/3 pyramidal neuron excitability during a late phase of critical period plasticity. *J. Neurosci.* **33**, 8810–8819 (2013).
29. M. S. Grubb, J. Burrone, Activity-dependent relocation of the axon initial segment fine-tunes neuronal excitability. *Nature* **465**, 1070–1074 (2010).
30. E. Campanac *et al.*, Enhanced intrinsic excitability in basket cells maintains excitatory-inhibitory balance in hippocampal circuits. *Neuron* **77**, 712–722 (2013).
31. T. Toyoizumi, M. Kaneko, M. P. Stryker, K. D. Miller, Modeling the dynamic interaction of Hebbian and homeostatic plasticity. *Neuron* **84**, 497–510 (2014).
32. J. P. Pfister, W. Gerstner, Triplets of spikes in a model of spike timing-dependent plasticity. *J. Neurosci.* **26**, 9673–9682 (2006).
33. J. Gjorgjieva, C. Clopath, J. Audet, J. P. Pfister, A triplet spike-timing-dependent plasticity model generalizes the Bienenstock-Cooper-Munro rule to higher-order spatiotemporal correlations. *Proc. Natl. Acad. Sci. U.S.A.* **108**, 19383–19388 (2011).
34. P. Znamenskiy *et al.*, Functional selectivity and specific connectivity of inhibitory neurons in primary visual cortex. bioRxiv DOI: http://dx.doi.org/10.1101/294835 (4 April 2018).
35. C. N. Levelt, M. Hübener, Critical-period plasticity in the visual cortex. *Annu. Rev. Neurosci.* **35**, 309–330 (2012).
36. T. Rose, J. Jaepel, M. Hübener, T. Bonhoeffer, Cell-specific restoration of stimulus preference after monocular deprivation in the visual cortex. *Science* **352**, 1319–1322 (2016).
37. M. Kaneko, J. Hanover, P. England, M. Stryker, TrkB kinase is required for recovery, but not loss, of cortical responses following monocular deprivation. *Nat. Neurosci.* **11**, 497–504 (2008).
38. T. P. Vogels, L. F. Abbott, Signal propagation and logic gating in networks of integrate-and-fire neurons. *J. Neurosci.* **25**, 10786–10795 (2005).
39. B. Van Vugt *et al.*, The threshold for conscious report: Signal loss and response bias in visual and frontal cortex. *Science* **360**, 537–542 (2018).
40. S. J. Barnes *et al.*, Subnetwork-specific homeostatic plasticity in mouse visual cortex in vivo. *Neuron* **86**, 1290–1303 (2015).
41. G. K. Ocker, B. Doiron, Training and spontaneous reinforcement of neuronal assemblies by spike timing plasticity. *Cerebr. Cortex* **29**, 937–951 (2018).
42. A. Maffei, K. Nataraj, S. B. Nelson, G. G. Turrigiano, Potentiation of cortical inhibition by visual deprivation. *Nature* **7**, 81–84 (2006).
43. J. M. Auth, T. Nachstedt, C. Tetzlaff, The interplay of synaptic plasticity and scaling enables self-organized formation and allocation of multiple memory representations. bioRxiv DOI: http://dx.doi.org/10.1101/260950 (14 October 2018).
44. J. Humble, K. Hiratsuka, H. Kasai, T. Toyoizumi, Intrinsic spine dynamics are critical for recurrent network learning in models with and without autism spectrum disorder. *Front. Comput. Neurosci.* **13**, 38 (2019).
45. F. Zenke, E. J. Agnes, W. Gerstner, Diverse synaptic plasticity mechanisms orchestrated to form and retrieve memories in spiking neural networks. *Nat. Commun.* **6**, 6922 (2015).
46. Y. Sweeney, S. J. Barnes, C. Clopath, Diverse homeostatic responses to visual deprivation by uncovering recurrent subnetworks. bioRxiv DOI: http://doi.org/10.1101/312926 (2 May 2018).
47. R. A. Crozier, Y. Wang, C. H. Liu, M. F. Bear, Deprivation-induced synaptic depression by distinct mechanisms in different layers of mouse visual cortex. *Proc. Natl. Acad. Sci. U.S.A.* **104**, 1383–1388 (2007).
48. C. Soares, K. F. Lee, J. C. Béïque, Metaplasticity at CA1 synapses by homeostatic control of presynaptic release dynamics. *Cell Rep.* **21**, 1293–1303 (2017).
49. G. LeMasson, E. Marder, L. Abbott, Activity-dependent regulation of conductances in model neurons. *Science* **259**, 1915–1917 (1993).
50. G. Turrigiano, G. LeMasson, E. Marder, Selective regulation of current densities underlies spontaneous changes in the activity of cultured neurons. *J. Neurosci.* **15**, 3640–3652 (1995).
51. L. A. Cingolani,*et al.*, Activity-dependent regulation of synaptic AMPA receptor composition and abundance by β3 integrins. *Neuron* **58**, 749–762 (2008).
52. S. J. Barnes *et al.*, Deprivation-induced homeostatic spine scaling in vivo is localized to dendritic branches that have undergone recent spine loss. *Neuron* **96**, 871–882 (2017).
53. Z. Ma, G. G. Turrigiano, R. Wessel, K. B. Hengen, Cortical circuit dynamics are homeostatically tuned to criticality in vivo. *Neuron* **104**, 655–664 (2019).
54. F. Zenke, G. Hennequin, W. Gerstner, Synaptic plasticity in neural networks needs homeostasis with a fast rate detector. *PLoS Comput. Biol.* **9**, e1003330 (2013).
55. R. Brette, Generation of correlated spike trains. *Neural Comput.* **21**, 188–215 (2009).
56. T. P. Vogels, H. Sprekeler, F. Zenke, C. Clopath, W. Gerstner, Inhibitory plasticity balances excitation and inhibition in sensory pathways and memory networks. *Science* **334**, 1569–1573 (2011).
57. J. A. D'amour, R. C. Froemke, Inhibitory and excitatory spike-timing-dependent plasticity in the auditory cortex. *Neuron* **86**, 514–528 (2015).
58. P. J. Sjöström, G. G. Turrigiano, S. B. Nelson, Rate, timing, and cooperativity jointly determine cortical synaptic plasticity. *Neuron* **32**, 1149–1164 (2001).
59. L. Montangie, C. Miehl, J. Gjorgjieva, Autonomous emergence of connectivity assemblies via spike triplet interactions. *PLoS Comput. Biol.* **16**, e1007835 (2020).
60. I. R. Fiete, W. Senn, C. Z. Wang, R. H. Hahnloser, Spike-time-dependent plasticity and heterosynaptic competition organize networks to produce long scale-free sequences of neural activity. *Neuron* **65**, 563–576 (2010).